Numerical Simulations and Analyses of Temperature Control Loop Heat Pipe for Space CCD Camera

MENG Qingliang*, YANG Tao, LI Chunlin

Beijing Institute of Space Mechanics & Electricity, Beijing 100094, China

As one of the key units of space CCD camera, the temperature range and stability of CCD components affect the image's indexes. Reasonable thermal design and robust thermal control devices are needed. One kind of temperature control loop heat pipe (TCLHP) is designed, which highly meets the thermal control requirements of CCD components. In order to study the dynamic behaviors of heat and mass transfer of TCLHP, particularly in the orbital flight case, a transient numerical model is developed by using the well-established empirical correlations for flow models within three dimensional thermal modeling. The temperature control principle and details of mathematical model are presented. The model is used to study operating state, flow and heat characteristics based upon the analyses of variations of temperature, pressure and quality under different operating modes and external heat flux variations. The results indicate that TCLHP can satisfy the thermal control requirements of CCD components well, and always ensure good temperature stability and uniformity. By comparison between flight data and simulated results, it is found that the model is to be accurate to within 1°C. The model can be better used for predicting and understanding the transient performance of TCLHP.

Keywords: Loop heat pipe, Temperature control, Numerical simulation and analyses, Heat and mass transfer, Space CCD camera

Introduction

Space CCD camera has been used in a wide range of fields, including military reconnaissance, resources exploration, surveying and mapping etc. [1] As one of the key units, the temperature range and stability of CCD components affect the image's indexes of signal-to-noise ratio and geometric accuracy directly or indirectly [2-4]. For some high performance camera, traditional products, limited by the heat transfer capacity, mounting dimensions and temperature stability, are not suitable for the thermal control of CCD components [5]. Reasonable thermal design and robust thermal control devices are needed.

LHP is an advanced heat transfer device, which uses the capillary pressure generated in a porous structure to circulate the working fluid from heat source to heat sink [6-7]. For the purpose of precise thermal control of CCD components, one kind of TCLHP is designed. By decoupling the evaporator and heat source, the capillary force is generated by loading heat directly on the evaporator, which force drives the fluid to absorb the heat produced by CCD components and release it through condensers. Compared with the traditional use of LHP, TCLHP has the characteristics of well start-up, good stability and flexible piping layout, which is promising in the thermal control of CCD components.

Extensive ground and flight tests have demonstrated

Nomenclature

Symbols

A	area (m^2)
c_p	specific heat at constant pressure (J/(kg·°C))

Greek symbols

Δ	difference
γ	latent heat of vaporization (kJ/kg)

D	diameter (m)	μ	dynamic viscosity (Pa·s)
G	heat conductivity (W/K)	ρ	density (kg/m^3)
h	convective heat transfer coefficient (W/(m^2·°C))	**Subscripts/superscripts**	
k	heat conductivity (W/(m·°C))	*accu*	accumulator
K	permeability (m^2)	*cw*	capillary wick
L	length (m)	*e*	evaporator
$\dot{m}$	mass flow (kg/s)	*env*	environment
Nu	Nusselt number	*f*	fluid
P	Pressure (N/m^2)	*i*	inner
Pr	Prandtl number	*l*	liquid
Q	heat load (W)	*o*	outer
r	radius (m)	*sat*	saturated
Re	Reynolds number	*vg*	vapor groove
T	temperature (°C)	*w*	wall
u	velocity (m/s)		
x	quality		

the excellent heat transfer performance of LHP [8]. However, compared with the experimental investigations, only a few studies on the theoretical analyses and mathematical modeling of LHP have been conducted so far. Accurate LHP model is needed to study the thermal performance, particularly in the orbital transients. The LHP system involves complex heat and mass transfer processes, rendering the mathematical modeling highly challenging. A number of steady-state models with varying levels of complexity have been proposed, which prove to be useful in predicating steady-state performance characteristics. Kaya et al. [9] developed a one dimensional (1D) mathematical model of LHP, which could reflect the variable conductance characteristics, but the oversimplification in the model brought large difference between the modeling and experimental results. A 1D steady-state model based on the energy balance equation, thermodynamic relationships and heat transfer and pressure drop calculations was developed by Chuang [10]. Improvement included the pressure drop induced by the bends, the convective heat transfer in the vapor grooves and heat fluxes in the wick. Adoni et al. [11] established a model to study the thermal and hydraulic performance of LHP, by using the mass and energy equations in the system. Additionally, the pressure drop across the capillary wick is calculated by the Darcy's law. Bai et al. [12] developed a model to study the effect of a two-layer compound wick, based on the energy conservation equations and empirical correlations. Rivière et al. [13] modeled a LHP based on the classic nodal network to study the fluid distribution in a loop.

Only a few of mathematical models have been established to study the transient behaviors in response to the power or sink cycles. For example, Wrenn et al. [14] and Hoang and Ku [15] developed a transient model based on 1D time-dependent conservation equations, which was an extension of transient model of capillary pumped loop (CPL). There were large errors between simulation and experimental results. Pouzet et al. [16] presented a comprehensive mathematical model, where the whole dynamic behaviors of a CPL due to power steps were successfully captured. Their model is helpful for the transient simulation of a LHP. Cullimore and Baumann [17] developed an advanced node-type LHP model written by FORTRAN code, which was embedded into Sinda/Fluint analyzer. This model is used by several researchers, such as in Refs. [18] and [19]. Compared with the test results, the predicted temperature showed little differences (less than 1°C). For the aspect of orbital simulation, Ferrandi et al. [20] established a transient model to design and simulate the thermal control system of LHP by Sinda/Fluint analyzer, which is used for the cooling of the cryomagnet avionics box on the Alpha Magnetic Spectrometer (AMS-02). Xin et al. [21] built a system LHP level for the thermal control of cryocooler on AMS-02, to analyze the transient performances due to the orbital change environment, and to understand the operation of LHP during the mission time. In any case, it is capable of aiding system design and predicating the working performance on orbit by LHP models based on the Sinda/Fluint code.

In this study, a transient mathematical model of TCLHP is established by using Sinda/Fluint code. In the following, the operating principle and mathematical model are presented first, followed by numerical results and discussions and comparison between flight data and

simulated results. Finally, some conclusions are drawn.

Analysis and Modeling

Operating principle

For the purpose of heat dissipation and temperature control of multi heat sources on the space CCD camera, the flow schematic of TCLHP is shown in Fig. 1. The operating principle is as follows. As heat is applied to the evaporator, liquid is vaporized and the capillary force is developed to push the vapor out of the evaporator. Vapor condenses into liquid in the condenser A and the capillary force continues to push liquid into the pre-heater, in which the fluid is changed into two phase fluid. Then the saturated fluid is forced into the cold plates and heat produced by CCD components is absorbed by the latent

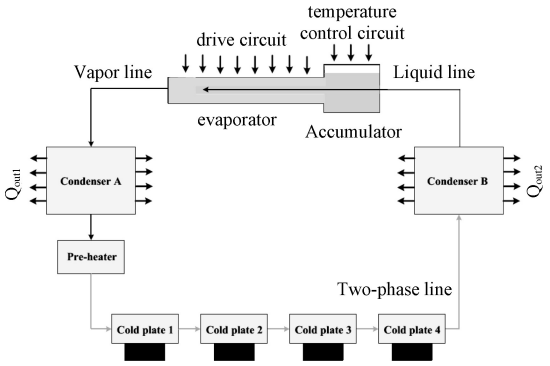

Fig. 1 The flow schematic of TCLHP

heat while the temperature keeps near constant. Two-phase fluid condenses into sub-cooled liquid again in the condenser B and the capillary force pushes it into the accumulator. And that cycle repeats.

Because the saturation states of fluid that in cold plates and accumulator are related, the following condition must be satisfied [8]:

$$T_{CCD} - T_{accu} = \frac{\Delta P_{CCD-accu}}{(dP/dT)_{sat}} \tag{1}$$

where T_{CCD} and T_{accu} are the saturation temperature of the fluid in cold plates and accumulator, $\Delta P_{CCD-accu}$ is the saturation pressure difference between cold plate and accumulator, and $(dP/dT)_{sat}$ is the slope of the pressure-temperature saturation line at T_{accu}. Eq. (1) states that, for a given pressure difference between these two elements, a saturation temperature difference corresponding must also exist. Generally, the number values of $(dP/dT)_{sat}$ are relative large. For example, the value of $(dP/dT)_{sat}$ at 5°C is 3.78 kPa/°C. For TCLHP, the mass flux is small and the tubes are smooth, so the pressure difference is small. If the number value of $\Delta P_{CCD-accu}$ is 1 kPa, the temperature difference is only 0.26°C according to Eq. (1). Hence, the working temperature of CCD components can be controlled by stabilizing the temperature of accumulator.

Mathematical Model

The evaporator and accumulator

The schematics and thermal network of evaporator and accumulator are shown in Fig. 2. Since the accumulator is integrated with the evaporator, there are complicated relations of heat and mass transfer between them.

The heat loaded on the evaporator wall is divided into three parts. The first part is from evaporator wall to the wet wick in evaporator by convective heat transfer, as shown by

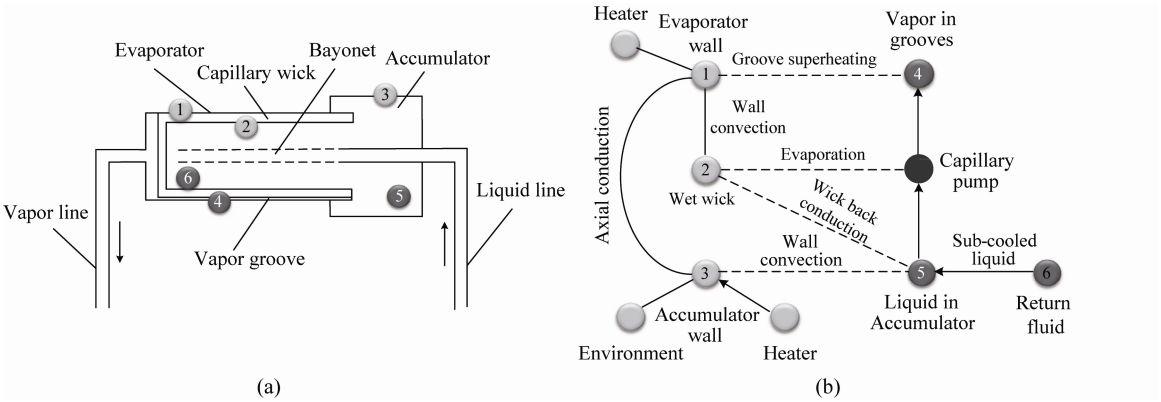

Fig. 2 The schematics of evaporator and accumulator (a), and the thermal network (b)

$$Q_{in1} = R \cdot (\pi h_e D_e L_e) \cdot (T_{w,e} - T_{f,e}) \tag{2}$$

with R an empirical constant that accounts for the heat transfer in the wick. The resulting value for R is a combination of conduction, convection, boiling, and evaporation between the wet wick and the evaporator wall [22].

This part also splits into an evaporation power and the back-conduction into the accumulator.

The evaporation power can be calculated by

$$Q_{in11} = \gamma \cdot \dot{m} \tag{3}$$

The back-conduction power from wet wick to accumulator is given by [12]

$$Q_{in12} = \frac{\dot{m} c_{pl}}{\left(D_{o,cw}/D_{i,cw}\right)^{\eta} - 1} \times \left(T_{f,e} - T_{f,\mathrm{accu}}\right) \tag{4}$$

where

$$\eta = \frac{\dot{m} c_{pl}}{2\pi k_e L_{cw}} \tag{5}$$

This section of part is related with the properties of capillary wick and working fluid and the mass flux.

The other two parts of heat are radial heat leak from the evaporator to the accumulator and the heat used for the superheating the vapor in grooves. Thus,

$$Q_{in2} = \frac{k_{accu} A}{L}\left(T_{w,e} - T_{w,\mathrm{accu}}\right) \tag{6}$$

$$Q_{in3} = h_{v,e} A \left(T_{w,e} - T_{w,vg}\right) \tag{7}$$

The thermal balance equation of accumulator satisfies the following relation:

$$Q_{accu} + Q_{in12} + Q_{in2} = Q_{env} + Q_{sub} \tag{8}$$

where Q_{accu} is the power of temperature control loaded on the accumulator, and Q_{env} and Q_{sub} can be calculated by

$$Q_{env} = G_{env}\left(T_{w,accu} - T_{env}\right) \tag{9}$$

$$Q_{sub} = \dot{m} c_{pl}\left(T_{f,accu} - T_{l,sub}\right) \tag{10}$$

Transport tubes

The transport tubes of TCLHP are usually small diameter smooth pipes with long transport length. By neglecting the heat exchange between tubes and environment, the energy conservation equation of the working fluid in lines can be written as [12]:

$$-\dot{m} c_{pl} \frac{dT}{dL} = \left(\frac{1}{h_i \pi d_i} + \frac{\ln\left(D_o/D_i\right)}{2\pi k_{cw}}\right)^{-1}\left(T_f - T_{env}\right) \tag{11}$$

The heat transfer coefficient at the inner wall can be calculated by

$$h_i = \frac{(Nu) k_f}{D_i} \tag{12}$$

Since there is large length-to-diameter ratio for the transport lines, the developed flow is assumed. Nu can be determined by the following equations:

$$Nu = \begin{cases} 4.36 & \mathrm{Re} < 1960 \\ \dfrac{(f/8)(\mathrm{Re}-1000)\,\mathrm{Pr}}{1+12.7(f/8)^{1/2}\left(\mathrm{Pr}^{2/3}-1\right)} & 1960 < \mathrm{Re} < 6420 \\ 0.023\,\mathrm{Re}^{0.8}\,\mathrm{Pr}^{n} & \mathrm{Re} > 6420 \end{cases} \tag{13}$$

where n is 0.4 when the pipe wall heats the fluid and n is 0.3 when the pipe wall cools the fluid.

The pressure drop in the transport lines can be calculated by

$$-\frac{dP}{dL} = f \times \frac{1}{2}\rho u^2 \times \frac{4}{D_i} \tag{14}$$

where the frictional factor is calculated as follows:

$$f = \begin{cases} 64/\mathrm{Re} & \mathrm{Re} < 2200 \\ 0.0791\,\mathrm{Re}^{-0.25} & 2200 < \mathrm{Re} < 10^5 \end{cases} \tag{15}$$

Two-phase flow model

Two-phase flow phenomena exist in pre-heater, CCD cold plate and condensers. The heat transfer coefficient of two-phase is related with the heat flux density, stability and flow pattern.

Shah correlation is used to calculate Nu as follows [23]:

$$Nu = 0.023\,\mathrm{Re}_l^{0.8}\,\mathrm{Pr}_l^{0.4}\left[(1-x)^{0.8} + \frac{3.8x^{0.76}(1-x)^{0.04}}{P^{*0.38}}\right] \tag{16}$$

where

$$Nu = \frac{h_{tp} d_e}{k_l} \tag{17}$$

$$\mathrm{Pr}_l = \frac{\mu_l c_{p_l}}{k_l} \tag{18}$$

$$P^* = \frac{P}{P_c} \tag{19}$$

The qualitative temperature in Eqs. (16)-(19) adopts the saturation temperature of two-phase section.

Capillary wick and vapor grooves

According to Darcy's law [24], the pressure drop through the capillary wick is determined by

$$\Delta P_{cwi} = \frac{\dot{m}\mu_l \ln\left(r_o/r_i\right)}{2\pi\rho_l K_{cwi} L_{cwi}} \tag{20}$$

The vapor is generated along the whole groove length, its mass flowrate increases approximately linearly along the vapor grooves. Hence, the effective length of vapor groove is approximated as half of its total length.

The pressure drop of vapor grooves can be calculated by Eqs. (14)-(15). In order to determine the Reynolds number, the hydraulic diameter of each vapor groove is used:

$$D_{h,vg} = \frac{2tw}{t+w} \tag{21}$$

where t and w are the height and width of the vapor groove, respectively.

Parameters and Conditions

Model Parameters

The working fluid is ammonia. The temperature of accumulator wall is controlled at 5°C during simulations. Table 1 shows the main parameters of each component.

The external heat flux variations and the working mode of CCD components

Fig. 3(a) shows the simulated external heat flux variations of condenser A and B. Fig. 3(b) gives the working mode of CCD components. The orbital period is 5852 s, and the operation period is 900 s. During operation, the power dissipation of each CCD component is 9 W, and the total heat power is 36 W.

Table 1 Model parameters

Components	Description
Capillary wick	Material: ceramic; Pore radius: 1×10^{-6} m; Porosity: 0.6
Evaporator	Material: stainless steel; Length: 0.13 m; OD: 0.014 m; Channels: 20
Accumulator	Material: stainless steel; Volume: 1.1×10^{-4} m^3
Condenser	Material: aluminum alloy; Area: 0.35 m^2 for condenser A, 0.33 m^2 for condenser B
Tubes	Material: stainless steel; OD: 0.003 m; ID: 0.002 m

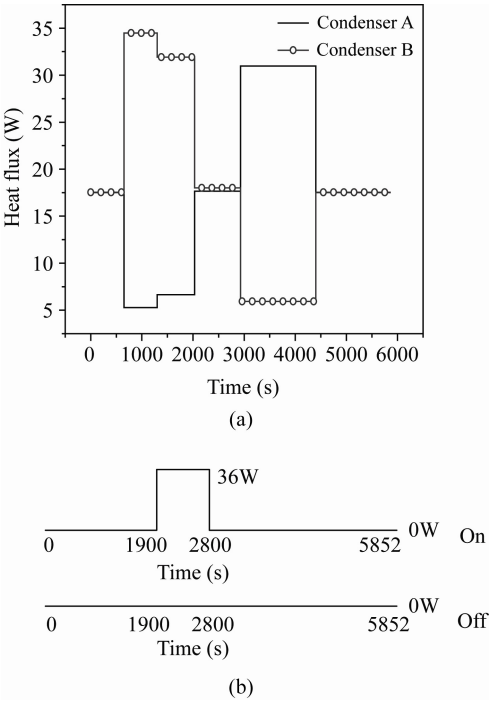

Fig. 3 The external heat flux variations of condenser A and B (a); the working mode of CCD components (b)

Results and Discussion

The temperature contour maps of condenser A and B, for cold case (a) and (b), and for hot case (c) and (d), are shown in Fig. 4. The cold case is corresponding to the time instant of the smallest external heat flux at the camera shut-down, and the hot case is corresponding to the time instant of the largest external heat flux during operation. In the application, the vapor line is coiled on the upper right section of the condenser B firstly, and then enters into the condenser A at which the fluid is sub-cooled enough. The working fluid is heated to be saturated in pre-heater. The two-phase fluid absorbs the heat produced by CCD components. The "hot" pipe is then coiled on the lower left of condenser B. After the working fluid changes to be sub-cooled again, it flows into the accumulator. The bulk temperature of condenser A and B is low in the cold case, while it is high in the hot case. With comparison of the four contour maps, it can be observed that the sections on which vapor and two-phase lines coiled are hot.

Fig. 5(a) and (b) show the temporal evolution of temperature and quality of working fluid in the pre-heater. The pre-heater is used to heat the sub-cooled liquid to saturated condition (i.e. set-point) before entering into the CCD cold plates. The numbers from 1 to 15 represent the fluid at different locations from the inlet to the outlet of pre-heater. Fig. 5(a) indicates that the external heat flux and working mode of CCD components affect the temperature of fluid in pre-heater. The temperature of outlet fluid is near 4.5°C after heated in pre-heater. Fig. 5(b) shows that the quality changes from 0 to 0.12−0.17, which means that the state of working fluid has changed

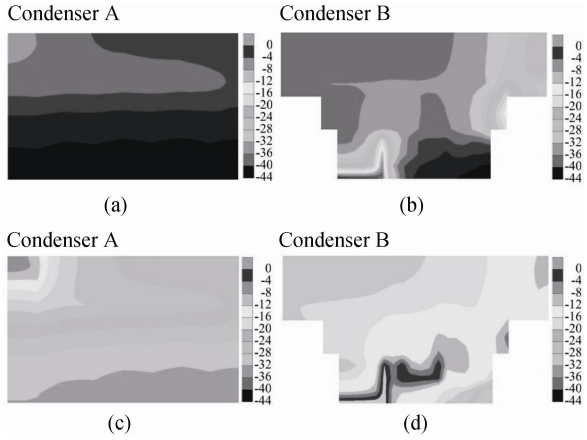

Fig. 4 The temperature contour maps of condenser A and B, for cold case (a) and (b), and for hot case (c) and (d)

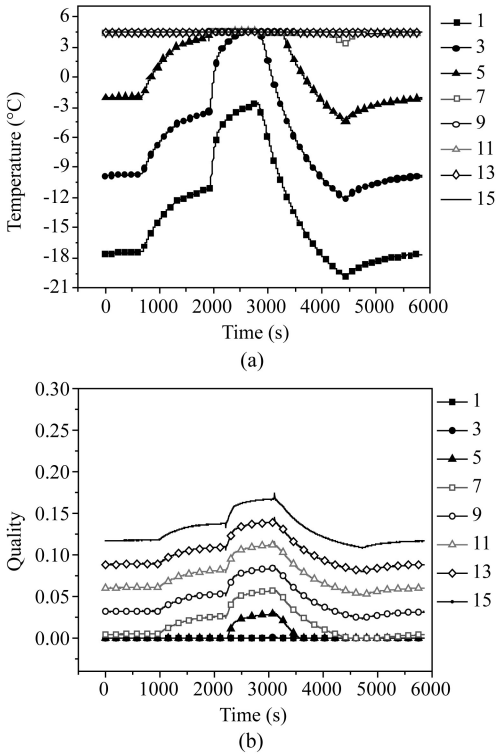

Fig. 5 The temporal evolution of temperature (a) and quality (b) of working fluid in pre-heater

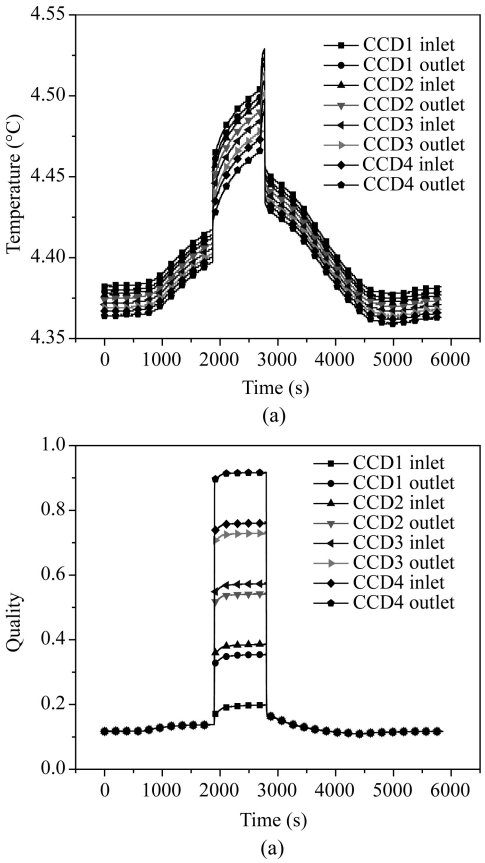

Fig. 6 The temporal evolution of temperature (a) and quality (b) of working fluid in CCD components

to be saturated. The pre-heater assures that the fluid flowing into CCD cold plate always keeps in two-phase condition during the mission time.

Fig. 6(a) and (b) give the temporal evolution of temperature and quality of working fluid in CCD components. After heated in pre-heater, the fluid that entering the cold plate becomes two-phase saturation state. During the camera shut-down period, the saturated fluid flows though the CCD cold plates in a near constant temperature. During operation period, the liquid in two-phase fluid is evaporated, and thus the quality increases. The temperature of fluid keeps in the range of 4.37−4.53°C, which provides a stabilized working boundary for CCD components. There is a decreasing temperature trend along the four cold plates due to the two-phase pressure drop. The temperature uniformity can be assured by the fluid characteristics of two-phase fluid. Unlike the temperature change, the quality changes obviously. The quality increases from 0.12 at the inlet of the first CCD cold plate to 0.90 at the outlet of the fourth CCD cold plate. The results indicate that the influences of external heat flux and working mode on temperature can be adjusted by the quality of two-phase fluid.

The profiles of temperature, pressure and quality of working fluid along flow distance, for cold case (a) and (b) and for hot case (c) and (d), are shown in Fig. 7. During the two cases, the temperature and quality decrease firstly, corresponding to that the vapor from evaporator becomes sub-cooled liquid. In order to save power, heat exchange between the sub-cooled and return two-phase lines occurs. Then the liquid flows into the pre-heater, and it turns into two-phase fluid. The temperature increases to a saturated point and the quality increase from zero to a number greater than zero. In cold case, the temperature and quality of two-phase fluid keep unchanged along the four CCD cold plates. In hot case, the temperature stays the same while the quality increases quickly along the heating elements. Saturated two-phase fluid condenses into sub-cooled liquid, and then it is pushed into the accumulator. The pressure is dropping along the flow direction.

Fig. 8 shows the comparison of average temperature of four CCD cold plates for the states of non-operation period (a) and operation period (b), between the data in orbit and the simulation results. During shut down period, CCD cold plates keep near 4.7°C in orbit, and the simulated temperature is around 4.4°C. The temperature difference between tests and simulation results is only 0.3°C. During operation, the average temperature of four CCD cold plates increases from 4.9°C to 5.5°C for flight results, and the temperature of them increases from 4.8°C

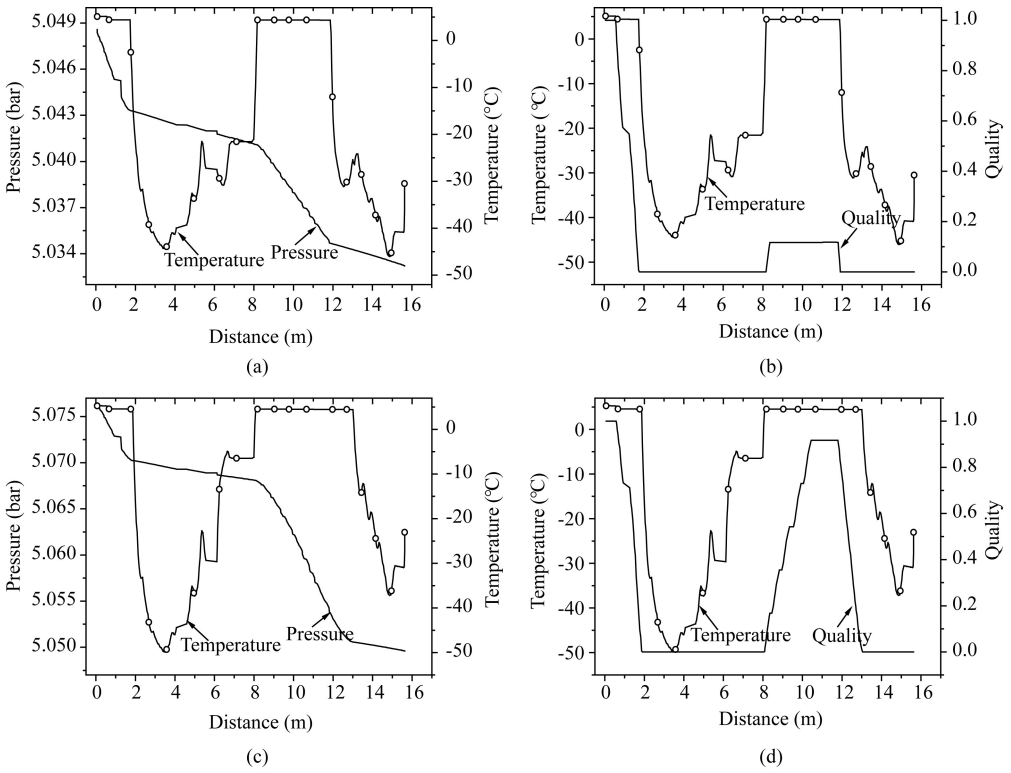

Fig. 7 Profiles of temperature, pressure and quality of working fluid along flow distance, for cold case (a) and (b) and for hot case (c) and (d)

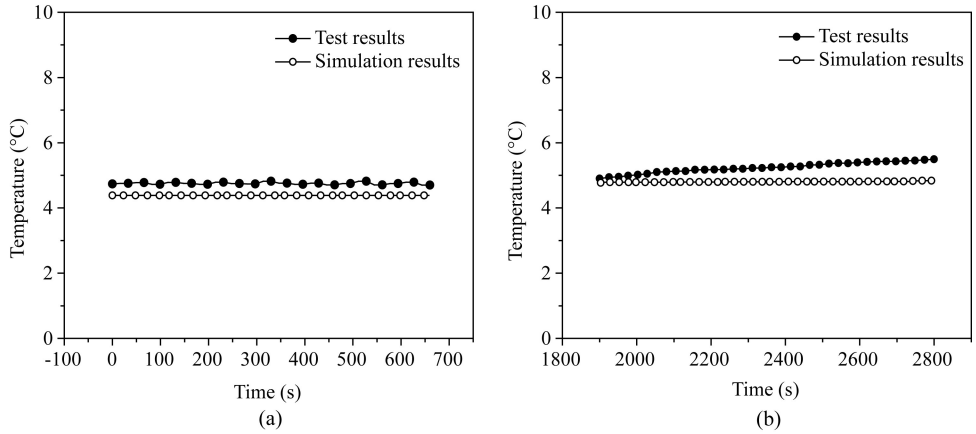

Fig. 8 The comparison of average temperature of four CCD cold plates for the states of non-operation period (a) and operation period (b)

to 4.9°C for simulation results. The temperature difference between the two cases is in the range of 0.1°C – 0.7°C. The model slightly under-predicts the loop operating temperature. The error between the model and the curve fit is generally less than 1°C, in many cases, less than 0.5°C, which verifies the validity and reasonability of TCLHP model. The model can be used for predicting the transient characteristics of LHP, and for understanding and analyzing the TCLHP's performance.

Conclusions

Numerical simulations have been carried out for a better understanding of the phenomena of heat and mass transfer for TCLHP of space CCD camera. The main conclusions from the numerical simulations are given as follows:

(1) The fluid flow states in the tubes coiled on the condensers affect the temperature distribution of con-

denser A and B. The temperature of the sections of vapor and two-phase lines coiled on is high, while the other sections are cold.

(2) The pre-heater between the condenser and CCD cold-plates assures that the fluid flowing into CCD cold-plate keeps in two-phase condition always during the mission time.

(3) The temperature of fluid in cold plates is stable and uniform. The influence of external flux and working mode on temperature can be adjusted by the quality of two-phase fluid.

(4) Comparison between flight data and simulated results indicates that the model slightly under-predicts the loop operating temperature and the error between the model and the curve fit is generally less than 1°C, in many cases, less than 0.5°C.

The results indicate that the temperature boundary of CCD components can be provided by the TCLHP, which can assure the CCD components working normally. The model can be better used for predicting and understanding the transient performance of TCLHP.

References

[1] Holst, G. C., 1996, *CCD Arrays, Cameras, and Displays*, JCD publishing, Bellingham (USA).

[2] LU, P., ZHAO, Z., YAN, Y., 2014, Precise Thermal Control of CCD in High Resolution Remote Sensing, Spacecraft Recovery & Remote Sensing, 35(4), 59–66.

[3] LI G., JIA, H., 2003, Thermal Analysis and Thermal Balance Test of CCD Assembly, Spacecraft Recovery & Remote Sensing, 24(3), 15–18.

[4] TONG, Y., LI, G., YU, L., et al., 2014, Heat Dissipation and Precise Temperature Control for High-power CCD Assembly, Spacecraft Recovery & Remote Sensing, 35(5), 46–53.

[5] Li C., 2014, Research on Space Optical Remote Sensor Thermal Control Technique, Journal of Astronautics, 35(8), 863–870.

[6] Maidanik, Y. F., Vershinin, S.V., Kholodov, V. F., et al., 1985, Heat Transfer Apparatus, United States Patent: 4515209.

[7] Kaya, T., Pérez, R., Gregori,C., et al., 2008, Numerical Simulation of Transient Operation of Loop Heat Pipes, Appli Therm Eng, 28, 967–974.

[8] Ku, J.T., 1999, Operating Characteristics of Loop Heat Pipes, in: 29th International Conference on Environmental System, No. 1999-01-2007, Denver, Colorado (USA).

[9] Kaya, T., Ku, J., Hoang, T. T., et al., 1999, Mathematical Modeling of Loop Heat Pipes, in: 37th AIAA Aerospace Sciences Meeting and Exhibit, No. 0477, Reno, Nevada (USA).

[10] Chuang, P., 2003, An Improved Steady-state Model of Loop Heat Pipes Based on Experimental and Theoretical Analyses (Ph. D. thesis), Pennsylvania State University, USA.

[11] Adoni, A., Ambirajan, A., Jasvanth,V., et al., 2007, Thermohydraulic Modeling of Capillary Pumped Loop and Loop Heat Pipe, J. Thermophy. Heat Transfer, 21, 410–421.

[12] Bai, L., Lin G., Zhang, H., et al., 2009, Mathematical Modeling of Steady-state Operation of a Loop Heat Pipe, Appl Therm Eng, 29, 2643–2654.

[13] Rivière, N., Sartre, V., Bonjour, J., 2010, Fluid Mass Distribution in a Loop Heat Pipe with Flat Evaporator, in: 15th International Heat Pipe Conference, Clemson, South Carolina (USA).

[14] Wrenn, K. R., Allen, R. D., Hoang, T. T., et al., 1999, Verification of a Transient Loop Heat Pipe Model, in: 29th International Conference on Environmental System, No. 1999-01-2010, Denver, Colorado (USA).

[15] Hoang, T. and Ku, J., 2003, Transient Modeling of Loop Heat Pipes, in: 1st International Energy Conversion Engineering Conference, No. AIAA-2003-6082, Portsmouth.

[16] Pouzet, E., Joly, J. L., Platel, V., et al., 2004, Dynamic Response of a Capillary Pumped Loop Subjected to Various Heat Load Transients, Int. J. Heat Mass Transfer, 47, 2293–2316.

[17] Cullimore, B. and Baumann, J., 2000, Steady State and Transient Loop Heat Pipe Modeling, in: 30th International Conference on Environmental Systems, No. 2000-01-2316, Toulouse, France.

[18] Rodriguez, J. I. and Pauken, M. T., 2000, Performance Characterization and Model Verification of a Loop Heat Pipe, in: 30th International Conference on Environmental Systems, No. 2000-01-2317, Toulouse, France.

[19] Hoff, C. J. and Rogers, P. D., 2000, Correlation of a Sinda/Fluint Model for a Switchbox Loop Heat Pipe, in: ASME National Heat Transfer Conference, No. 2000-12160, New York.

[20] Zinna, S., Marengo, M., Vasiliev, L., et al., 2009, Advanced Design of A Low Cost Loop Heat Pipe and Comparison with A Novel Numerical Approach, in: 41st AIAA Thermophysics Conference., San Antonio, TX.

[21] Xin, G., Cheng, Y., Luan, T., et al., 2009, Simulation of a LHP-based Thermal Control System under Orbital Environment, Appl. Therm. Eng., 29, 2726–2730.

[22] Liao, Q. and Zhao, T. S., 1999, Evaporative Heat Transfer in a Capillary Structure Heated by a Grooved Block, J. Thermophys. Heat Transfer, 13, 126–133.

[23] Friedel, L., 1979, Improved Friction Pressure Drop Correlation for Horizontal and Vertical Two-Phase Pipe Flow, in: European Two-Phase Flow Group Meeting, Paper E2, Ispra, Italy, pp. 1158–1162.

[24] Reay, D.A. and Kew, P. A., 2006, Heat Pipes, 5th edition, Butterworth-Heinemann, England.